*Journal of Machine Engineering, 2018, Vol. 18, No. 1, 61-71*
*ISSN 1895-7595 (Print) ISSN 2391-8071 (Online)*

Received: *3 January 2018*/ Accepted: *09 February 2018* / Published online: *12 March 2018*

*flow simulation,*
*emission of airborne sound,*
*acoustic examination*

H.-Christian MÖHRING[1*]
Thomas STEHLE[1]
Kamil GÜZEL[1]
Christoph ZIZELMANN[1]

# NUMERICAL FLOW SIMULATION OF ROTATING CIRCULAR SAW BLADES FOR THE INVESTIGATION OF SOUND GENERATION MECHANISMS

Emission of airborne sound in the production industry is endangering the employees' health and is lowering productivity. Circular saw blades in particular cause high sound pressure levels. Therefore, the tool geometry of saw blades should be improved in the sense that the emission of airborne sound is lowered. In this work, the basics for the tool optimization regarding the emission of airborne sound are elaborated. To avoid high costs for various prototypes and experimental investigations, a computational fluid dynamics (CFD) simulation is used. By this, the effects of the adjustments of the geometry on the fluid mechanics can be researched efficiently. Using the acoustic analogy of Ffowcs-Williams/Hawkings, the results of the numerical flow simulation are converted into the sound pressure level. To validate the calculated results, previously conducted experiments are used for comparison. The calculated results correspond well to the values from the experimental measurements. Hence, it is possible to use the developed method to predict the influence of geometry adjustments on the acoustic behaviour, making the optimization process possible. In an outlook, the concept for an optimization loop is explained, which couples the CFD simulation with a parameterized geometry model and an evaluation algorithm.

## 1. INTRODUCTION

With regard to the emergence of noise on rotating circular saw blades, there must be a distinction, whether the saw blade is running under load or idling. In operation, the acoustic emission is caused by vibrations of the circular saw blade as a result of the process forces occurring. At idle the noise is due to fluid mechanical effects on the tool [1]. On the one hand, it is due to the protruding saw teeth, which carry an overpressure field in front of them and drag a negative pressure field behind them. On the other hand, turbulent vortex shedding occurs on the rotating tool surface [2].

[1] University of Stuttgart, Institute for Machine Tools (IfW), Stuttgart, Germany
[*] E-mail: hans-christian.moehring@ifw.uni-stuttgart.de
DOI: 10.5604/01.3001.0010.8823

The reduction of the noise emission of circular saw blades has already been subject of numerous investigations. By introducing composite systems or damping materials, the noise emission could be reduced [3,4]. Other investigations dealt with the use of compressed air to have a positive influence on the flow conditions [2]. Various tool manufacturers use slots filled with polymers to reduce vibrations. Others cut thin slits on the steel blade by laser processing.

In this work, the approach is followed to adapt the chip space or tooth geometry so that the air flow processes can favorably influence the noise emission. For this adaptation, the method of computational aeroacoustics (CAA) is used. This means that the flow processes are calculated by using a numerical flow simulation. Subsequently, a conversion into sound quantities is carried out using the acoustic analogy of Lighthill and the extension of Ffowcs-Williams/Hawkings.

For the following optimization, a simulation model of an existing circular saw blade is first created and the results are compared to experimentally performed sound measurements. An outlook for the optimization of the tool geometry is shown afterwards.

## 2. EXPERIMENTAL MEASUREMENTS

In order to be able to validate the results of the simulation, sound measurements were carried out with a circular saw blade at different rotational speeds. The measurements took place in an acoustic laboratory with a sound-absorbing ceiling and walls. The test set-up and the measuring instruments used made it possible to measure according to accuracy class 2 (DIN 3744). Fig. 1 shows the test stand used for the performed sound measurements.

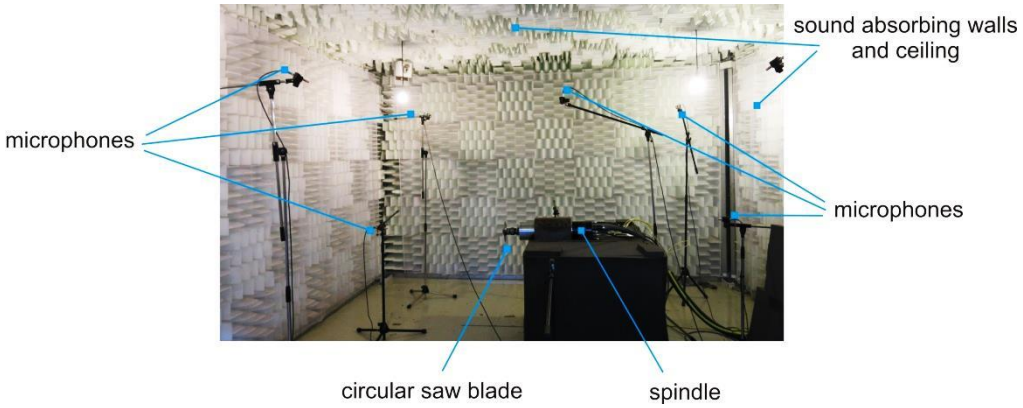


Fig. 1. Test stand of the experimental sound measurements

The measurements were carried out at rotational speeds of 2000, 3000, 5000 and 7000 $min^{-1}$. In each case, the sound pressure level in 1 m distance was determined. The results are shown in Table 1. It should be noted that no frequency-dependent evaluation of the sound pressure level was carried out during the sound measurements. Hence, the results could be compared with those of the simulations.

Table 1. Results of sound pressure level measurements

| Rotational speed [$min^{-1}$] | 2000 | 3500 | 5000 | 7000 |
|---|---|---|---|---|
| Sound pressure level [dB] | 67.05 | 74.86 | 77.64 | 84.12 |

## 3. SIMULATION

To carry out the simulation, the geometry of an exemplary circular saw blade was measured with a digital microscope and modeled using a CAD system. The circular saw blade used has a diameter of 160 mm and 36 teeth, which are arranged as alternating teeth (Fig. 2).

The flow simulation was performed using ANSYS CFX. In the simulation, the circular saw blade itself was not used. Rather, the saw blade was subtracted from a calculation volume and later considered in the setup as a frictional wall in the simulation (Fig. 2). The calculation volume has a diameter of 360 mm and a thickness of 90 mm.

The outside area of the calculation volume was taken into account as a frictional wall and the rotational speeds of the rotating calculation volume were set in the setup. For this purpose, the experimentally investigated rotational speeds were applied. Furthermore, different turbulence models were compared. These include the k-ε model, the Shear Stress Transport model (SST), the Baseline Reynolds Stress model (BSL) and the SSG Reynolds Stress model by Speziale, Sarkar and Gatski.

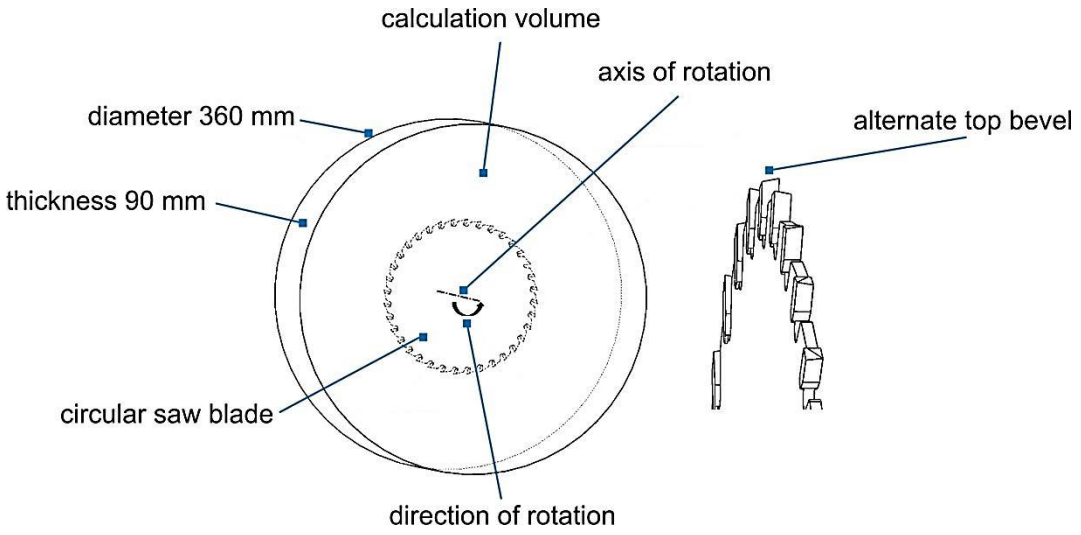


Fig. 2. CAD model of the calculation volume

Once completed, the results of the simulation can be displayed and viewed. In the present case, the direction of rotation of the calculation volume should be checked in the context of a plausibility check. The direction of rotation can be recognized by the pressure curve on the circular saw blade surface. Thus, overpressure must prevail on

the rake surface of the teeth and a negative pressure behind it must be formed. If the results are plausible, they can be exported to calculate the sound pressure level.

## 4. ACOUSTIC ANALOGY

The conversion of the results from the flow simulation is done by the acoustic analogy of Lighthill and the extension of Ffowcs-Williams/Hawkings [5-7].

The propagation of sound can generally be described by the wave equation. Lighthill was able to show that the basic equations of fluid mechanics (continuity and momentum equation) can be calculated in such a way that they can be converted into a wave equation. Consequently, it is possible to convert flows into sound parameters. The derived acoustic analogy can be seen in equation (1):

$$\begin{aligned}\frac{\partial^2\rho}{\partial t^2}-c_0^2\frac{\partial^2\rho}{\partial x_i^2}&=\frac{\partial\dot{m}}{\partial t}-\frac{\partial}{\partial x_i}\left(\rho f_i+\dot{m}v_i\right)+\frac{\partial^2}{\partial x_i\partial x_j}\left(\rho v_i v_j+p_{ij}-c_0^2\rho\delta_{ij}\right)\\&=\frac{\partial\dot{m}}{\partial t}-\frac{\partial}{\partial x_i}\left(\rho f_i+\dot{m}v_i\right)+\frac{\partial^2}{\partial x_i\partial x_j}T_{ij}\end{aligned} \tag{1}$$

where: $\rho$ is density, $t$ is time, $x_{i,j}$ is spatial directions, $\dot{m}$ is mass flow, $f_i$ is force, $v_i$ is velocity, $p$ is pressure, $c_0$ is speed of sound, $\delta_{ij}$ is Kronecker Delta [8].

To solve the above equation, the generalized Kirchhoff equation is used. Fig. 3 shows the schematic structure with the moving solid $S$ in the calculation volume $V$.

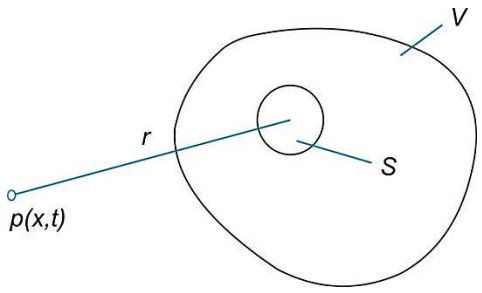


Fig. 3. Schematic structure for the solution of acoustic analogy using the generalized Kirchhoff equation

$$\begin{aligned}p(x,t)=&\int_V\frac{1}{4\pi r}\left(\frac{\partial\dot{m}}{\partial t}\right)_\tau dV-\int_S\frac{1}{4\pi r}\left(\frac{\partial(\rho v_i)}{\partial t}\right)_\tau n_i dS-\frac{\partial}{\partial x_i}\int_V\frac{1}{4\pi r}\left(f_i+\dot{m}v_i\right)_\tau dV\\&+\frac{\partial}{\partial x_i}\int_S\frac{1}{4\pi r}\left(\rho v_i v_j+p_{ij}\right)_\tau n_j dS+\frac{\partial^2}{\partial x_i\partial x_j}\int_V\frac{1}{4\pi r}\left(T_{ij}\right)_\tau dV\end{aligned} \tag{2}$$

where: $p(x,t)$ is pressure in receptor point, $r$ is distance, $\dot{m}$ is mass flow, $t$ is time, $\tau$ is elapsed time, $V$ is calculation volume, $\rho$ is density, $v_i$ is velocity, $n_{i,j}$ is normal vector, $S$ is surface, $x_{i,j}$ are spatial directions, $f_i$ is force, $p_{ij}$ is pressure tensor, $T_{ij}$ is Lighthill tensor [8].

The solution can be considerably simplified by making assumptions. First, the mass flow $\dot{m}$ is considered. In the present case, this would be a mass flow entering the calculation volume $V$ from the outside which is assumed to be $\dot{m} = 0$. The term $f_i$ represents an outside force acting on the calculation volume $V$ or a reaction force due to the mass flow. Both are not present in the current case, which is why they are omitted. This leads to the following results of the integrals

$$\int_V \frac{1}{4\pi r}\left(\frac{\partial \dot{m}}{\partial t}\right)_\tau dV = 0 \text{ and } \frac{\partial}{\partial x_i}\int_V \frac{1}{4\pi r}\left(f_i + \dot{m}v_i\right)_\tau dV = 0$$

For the remaining integrals further simplifications can be made. The pressure tensor $p_{ij}$ is calculated as follows:

$$p_{ij} = p\delta_{ij} - \tau_{ij} \tag{3}$$

where $p_{ij}$ is pressure tensor, $p$ is pressure, $\delta_{ij}$ is Kronecker Delta, $\tau_{ij}$ is shear stress tensor.

If a Newtonian medium is assumed, the shear stress is eliminated and only the following expression remains.

$$p_{ij} = p\delta_{ij} \tag{4}$$

If also a constant density and an isentropic medium is assumed at low Mach numbers and a high Reynolds number, the Lighthill tensor is simplified further. The Lighthill tensor without simplifications is calculated according to equation (5).

$$T_{ij} = \rho v_i v_j + \delta_{ij}\left[\left(p - p_0\right) - c_0^2\left(\rho - \rho_0\right)\right] - e_{ij} \tag{5}$$

where $T_{ij}$ is Lighthill tensor, $\rho$ is density, $v_{i,j}$ is velocity, $\delta_{ij}$ is Kronecker Delta, $p$ is pressure, $c_0$ is speed of sound, $e_{ij}$ is viscious stress tensor.

The above assumptions lead to the simpler form:

$$T_{ij} = \rho v_i v_j \tag{6}$$

One final assumption is made by neglecting the elapsed time. This would take the difference between the sound pressure level at the origin of the sound and the registration of the sound at the receptor point into account. Since the time difference is very small due to the short distance and the sound emission is also assumed to be stationary, this derivation is neglected.

In order to be able to calculate the sound pressure level, the required values have to be taken from the simulation. ANSYS CFX provides an export option for this purpose. As a result, the required pressure/velocity and their gradients can be obtained. These are

numerical values, which is why the integration and derivation must also be performed numerically.

For the solution of the Kirchhoff equation, relations were derived which result in the overall solution with the help of these exportable values. For the first integral, the following relation results:

$$\int_S \frac{1}{4\pi r}\left(\frac{\partial(\rho v_i)}{\partial t}\right)_\tau n_i dS = \frac{\rho}{4\pi r}\sum_n A_n\left(-v_{1n}\frac{\partial v_{1n}}{\partial x_1}n_{1n} - v_{2n}\frac{\partial v_{2n}}{\partial x_2}n_{2n} - v_{3n}\frac{\partial v_{3n}}{\partial x_3}n_{3n}\right) \tag{7}$$

where $S$ is surface, $r$ is distance, $\rho$ is density, $v_i$ is velocity, $n_i$ is normal vector, $A$ is area, $x_i$ is spatial direction.

Because the normal vectors are not perpendicular on the circular saw blade, but perpendicular on the calculation volume, negative signs appear in the solution. The time derivative of the velocity does not exist as an export option in ANSYS CFX. Therefore, the spatial gradient of the velocity is multiplied by the velocity to obtain the time derivative (acceleration). The solution of the integral is calculated using the discretized finite elements on the circular saw blade surface. The respective velocities and gradients are multiplied by the associated area and summed up for the entire area.

The solution of the next integral is shown in equation (8).

$$\frac{\partial}{\partial x_i}\int_S \frac{1}{4\pi r}\left(\rho v_i v_j + p_{ij}\right)_\tau n_j dS = \frac{1}{4\pi r}\sum_n A_n\left|\vec{a}_n\right| \tag{8}$$

where $x_i$ is spatial direction, $S$ is surface, $r$ is distance, $\rho$ is density, $v_i$ is velocity, $p_{ij}$ is pressure tensor, $n_j$ is normal vector, $A$ is area, $\vec{a}_n$ is vector.

The vector $a$ is composed at every point $n$ of the calculation volume according to the following equation. For the derivatives, the product rule (if necessary the summation rule) of the derivation must be considered. The norm can be calculated by the geometric addition of the individual components of the vector.

$$\vec{a}_n = \begin{pmatrix} -\left(2v_{1n}\rho\frac{\partial v_{1n}}{\partial x_1} + \frac{\partial p}{\partial x_1}\right)n_{1n} - \rho\left(\frac{\partial v_{1n}}{\partial x_1}v_{2n} + \frac{\partial v_{2n}}{\partial x_1}v_{1n}\right)n_{2n} - \rho\left(\frac{\partial v_{1n}}{\partial x_1}v_{3n} + \frac{\partial v_{3n}}{\partial x_1}v_{1n}\right)n_{3n} \\ -\rho\left(\frac{\partial v_{2n}}{\partial x_2}v_{1n} + \frac{\partial v_{1n}}{\partial x_2}v_{2n}\right)n_{1n} - \left(2v_{2n}\rho\frac{\partial v_{2n}}{\partial x_2} + \frac{\partial p}{\partial x_2}\right)n_{2n} - \rho\left(\frac{\partial v_{2n}}{\partial x_2}v_{3n} + \frac{\partial v_{3n}}{\partial x_2}v_{2n}\right)n_{3n} \\ -\rho\left(\frac{\partial v_{3n}}{\partial x_3}v_{1n} + \frac{\partial v_{1n}}{\partial x_3}v_{3n}\right)n_{1n} - \rho\left(\frac{\partial v_{3n}}{\partial x_3}v_{2n} + \frac{\partial v_{2n}}{\partial x_3}v_{3n}\right)n_{2n} - \left(2v_{3n}\rho\frac{\partial v_{3n}}{\partial x_3} + \frac{\partial p}{\partial x_3}\right)n_{3n} \end{pmatrix} \tag{9}$$

where $v_i$ is velocity, $\rho$ is density, $x_i$ is spatial direction, $p$ is pressure, $n_j$ is normal vector.

The signs are also opposite due to the reverse direction of the normal vectors. The integral is solved analogously to the previous one.

Equivalent to the Euclidean norm of a vector, the operation can also be performed on a matrix. By geometrical addition of all components, the so called Frobenius norm is formed. This operation is applied on the twice-differentiated Lighthill tensor (10).

$$\frac{\partial^2}{\partial x_i \partial x_j}\int_V \frac{1}{4\pi r}\left(T_{ij}\right)_\tau dV = \frac{1}{4\pi r}\sum_n V_n \sqrt{\sum_i \sum_j \left[A_{ijn}\right]^2} \tag{10}$$

where $x_{i,j}$ are spatial directions, $V$ is calculation volume, $r$ is distance, $T_{ij}$ is Lighthill tensor, $[A_{ij}]$ is component of Lighthill tensor.

The matrix [A] at each point $n$ of the calculation volume is calculated according to the following expression. Attention must be paid to the application of the product rule of derivation. For reasons of clarity, the extensive form of the calculated terms is not displayed.

$$[A_n] = \begin{pmatrix} \left(\frac{\partial^2\left(\rho v_{1n}^2\right)}{\partial x_1^2}\right) & \left(\frac{\partial^2\left(\rho v_{1n} v_{2n}\right)}{\partial x_1 \partial x_2}\right) & \left(\frac{\partial^2\left(\rho v_{1n} v_{3n}\right)}{\partial x_1 \partial x_3}\right) \\ \left(\frac{\partial^2\left(\rho v_{2n} v_{1n}\right)}{\partial x_2 \partial x_1}\right) & \left(\frac{\partial^2\left(\rho v_{2n}^2\right)}{\partial x_2^2}\right) & \left(\frac{\partial^2\left(\rho v_{2n} v_{3n}\right)}{\partial x_2 \partial x_3}\right) \\ \left(\frac{\partial^2\left(\rho v_{3n} v_{1n}\right)}{\partial x_3 \partial x_1}\right) & \left(\frac{\partial^2\left(\rho v_{3n} v_{2n}\right)}{\partial x_3 \partial x_2}\right) & \left(\frac{\partial^2\left(\rho v_{3n}^2\right)}{\partial x_3^2}\right) \end{pmatrix} \tag{11}$$

where $[A_n]$ is twice-differentiated Lighthill tensor, $\rho$ is density, $v_i$ is velocity, $x_i$ is spatial direction.

The overall result is built by adding up the integrals to the sound pressure in the receptor point *p(x,t)*. In order to obtain the sound pressure level, it has to be calculated according to equation (12).

$$L_p = 20 \cdot \log_{10}\left(\frac{p(x,t)}{2 \cdot 10^{-5} Pa}\right) dB \tag{12}$$

where $L_p$ is sound pressure level, *p(x,t)* is sound pressure in receptor point.

The diagram in Fig. 4 shows the calculated sound pressure levels over the rotational speed. The comparison of the used turbulence models with the experimentally measured values can also be seen.

All turbulence models correspond to the trend of the sound pressure level of the experiment. A logarithmic function was chosen for the balance line since the sound pressure level is based on a logarithmic function. The calculated sound pressure levels are clearly above the measured values. There are multiple reasons for these differences. Due to production tolerance, the CAD model is not an exact representation of the saw blade. Also, numerical simulations always have a residual error. Furthermore, the simulation uses turbulence models, which don't exactly calculate the actual occuring turbulences.

For the optimization of circular saw blades a tendenctious course like in the experiment, however, is sufficient. The SSG Reynolds Stress model provides the most

accurate result, because the balance line is shifted upwards almost parallel. This becomes clear when regarding the formulas of the balance lines of the SSG Reynolds Stress model and the measurement in Fig. 4.

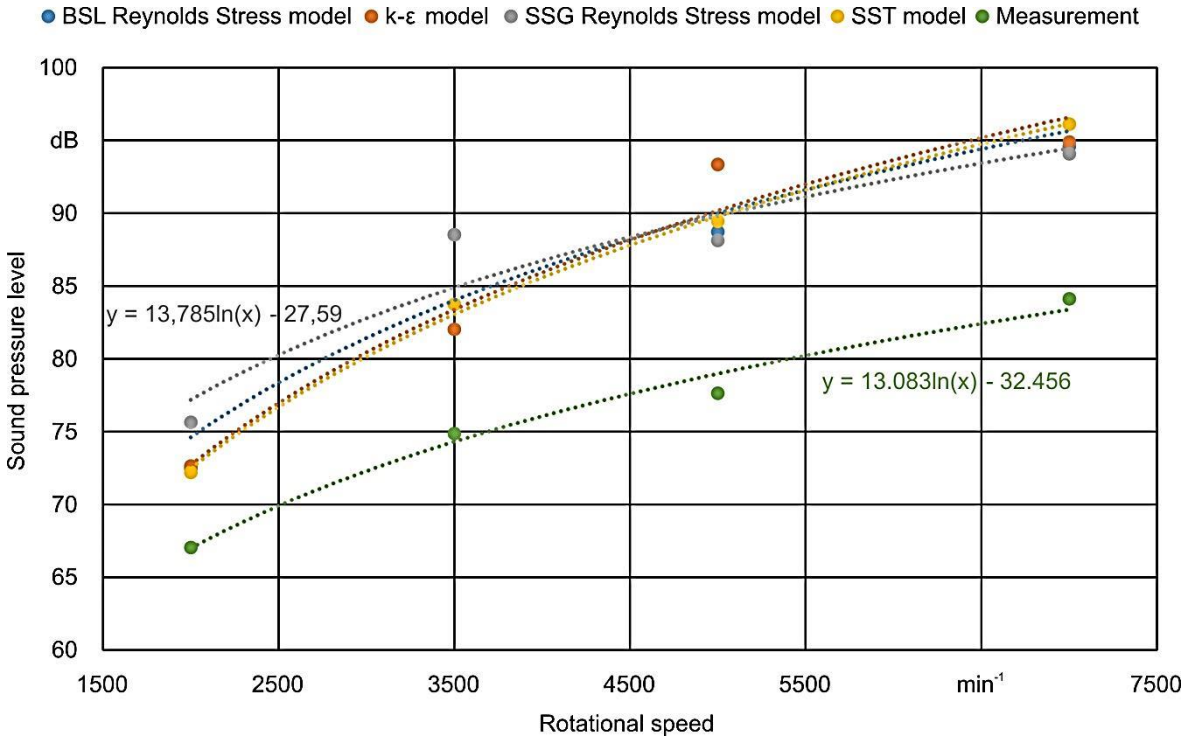


Fig. 4. Comparison of sound pressure levels at different rotational speeds and turbulence models

In order to save computing capacity, the rotational periodicity of the tool was exploited. For the circular saw blade with 36 teeth, a circle section of 40° was chosen, so that several chip spaces were considered. In general the symmetry to the middle plane could also be exploited - due to the alternate top bevel design it wasn't used. In order to be able to compare the results the same dimensions for the calculation volume were used. The results were multiplied by nine, since only one-ninth of the tool was calculated. The diagram in Fig. 5 shows the results of this simplification.

In comparison to the 360° simulation the slopes of the curves have changed. In the lower rotational speed range, the results of the simulation are closer to the experiment. With increasing rotational speeds the deviations increase as well. These can be explained by the factorization. The turbulence models ensure an uneven distribution of turbulence in the calculation volume. This can be clearly seen when looking at the streamlines in the following Fig. 6.

Since only one-ninth of the total volume is calculated, nine areas of repetitive turbulence are created across the volume. Furthermore, the model is meshed differently. This also causes deviations. The deviations in the slopes of the sound pressure level curves depend on the turbulence model. For the optimization, the analysis of the section of the circle is still suitable, since this is a comparitive study. This means, that only

the relative changes of the sound pressure levels can be applied as optimization criterion, rather than the absolute values. Due to the shorter computing time, the process can be considerably accelerated.

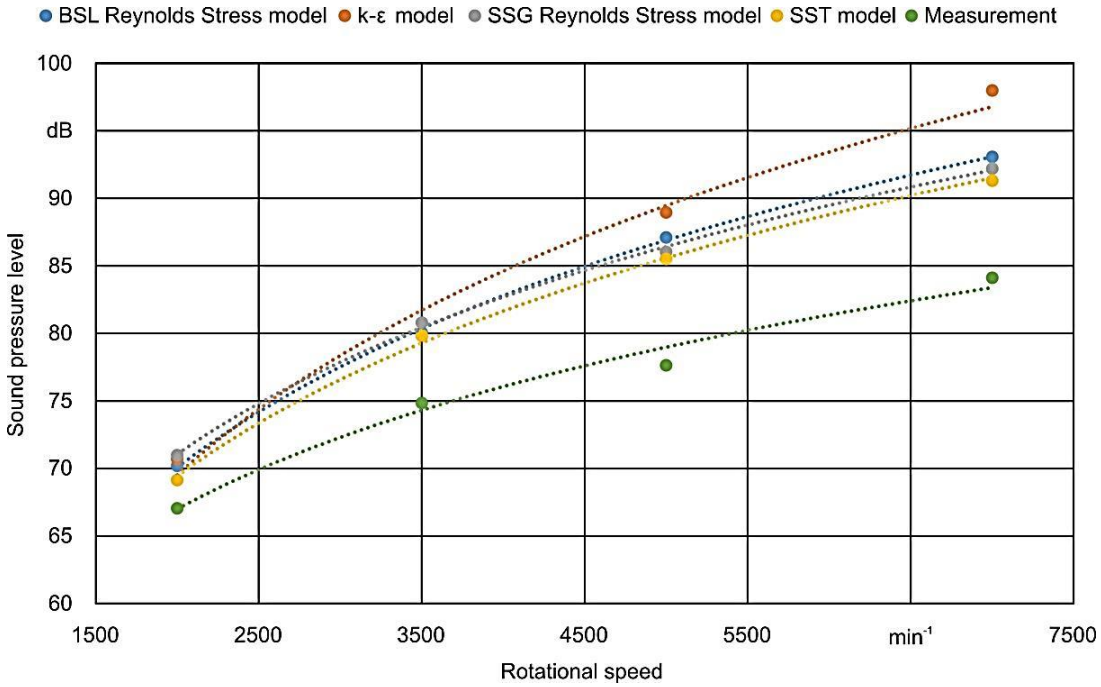


Fig. 5. Comparison of the sound pressure level of the 40° model

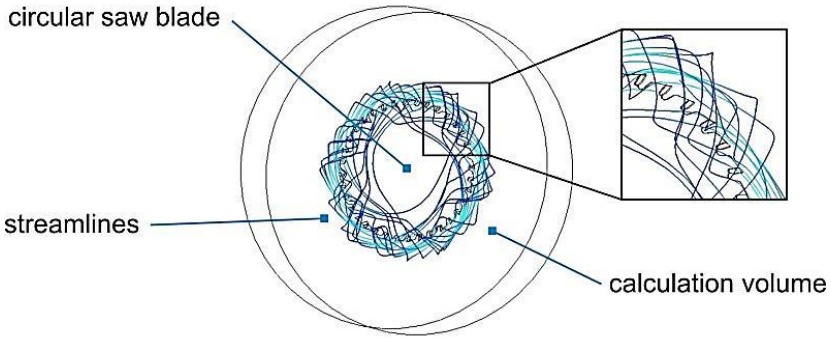


Fig. 6. Streamlines in the calculation volume at 2000 $min^{-1}$ using the k-ε model

## 5. SUMMARY AND FUTURE RESEARCH

With the performed simulations, it is now possible to predict the acoustic behavior of the saw blade with sufficient accuracy. The trend of the dependence of the sound pressure level on the rotational speed was shown for the used circular saw blade. Thus, the foundation for the optimization of the saw blade geometry in regards to the noise emission is elaborated.

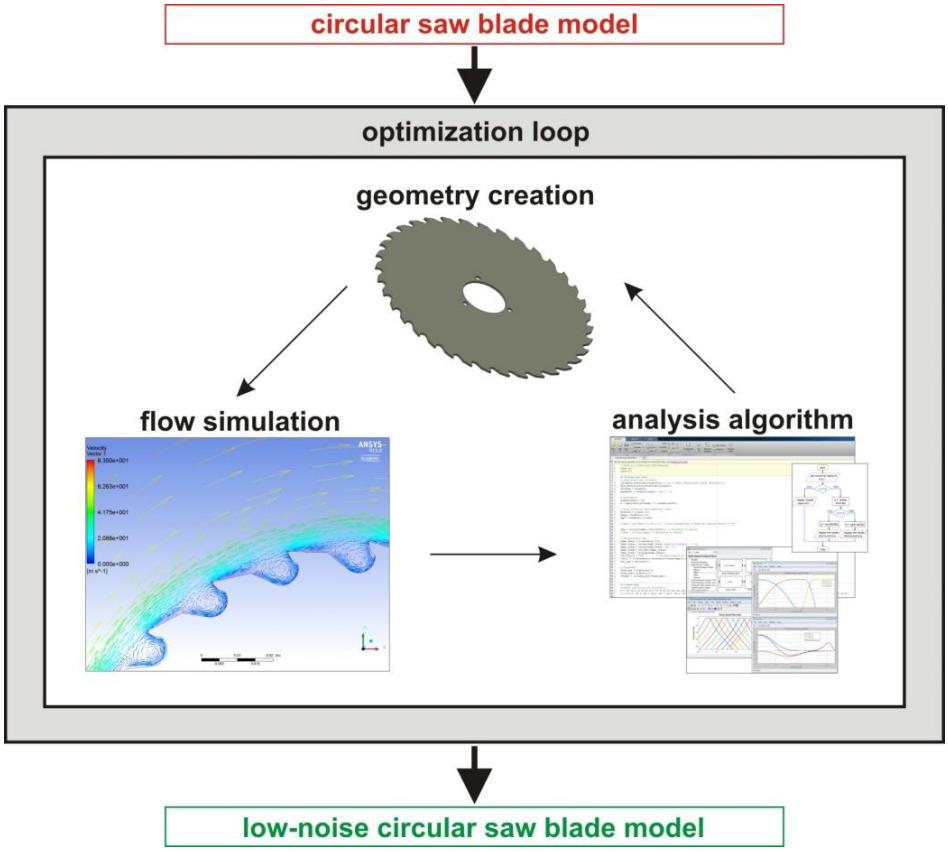


Fig. 7. Numerical optimization process for the design of low-noise circular saw blade geometries

As part of ongoing work, a numerical optimization process is currently developed for the design of low-noise circular saw blade geometries, as shown in Fig. 7. The optimization loop consists of a coupling of a parameterized CAD model, the flow simulation and an evaluation algorithm. The parameterized CAD model is intended to be defined by fixed parameters such as the saw blade thickness and diameter and variable parameters such as chip space radius and tooth backlash length.

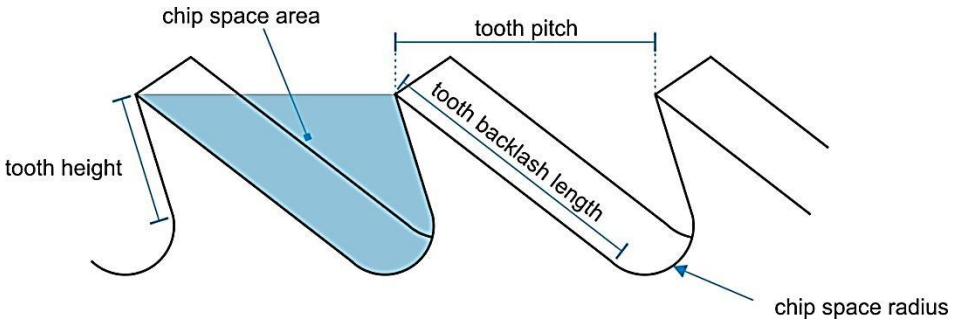


Fig. 8. Variable geometry parameters of the CAD model

The strategy of the algorithm is to vary these variable parameters (Fig. 8) either individually or in combination, with the goal of reducing the sound pressure level to a set

value. As a boundary condition, a minimum area of the chip space must be specified. Otherwise, the computational effort would be too high and the end result would always be a model without a chip space (circular blank).

The minimum size of the chip space is derived from the results of previous studies [9]. As part of these experiments, the influence of various tool/process parameters and materials on the chip loosening factor were investigated. The chip loosening factor describes the relation between the original volume of the material and the volume of the chip material. In general, the larger the chip loosening factor, the more space the chip will take. As a result, the chip spaces of the saw blade must be larger, which in turn can lead to an increase in the sound pressure level.

This optimization methodology can be applicable in tool development for wood, metal and composite machining.

## ACKNOWLEDGEMENTS

*The authors would like to thank the German Research Foundation (DFG) for the financial and organizational support of this project. The results presented in this paper were obtained within the DFG-project "Low-Noise Saw Blades for Timber and Derived Timber Working" STE 1563/5-1.*

## REFERENCES

[1] KUOLT H., 2006, *Geräuschentstehung und Maßnahmen zur Lärmminderung an Holzbearbeitungsmaschinen*, Dissertation Universität Stuttgart.

[2] HEISEL U., STEHLE T., 2013, *Entwicklung einer auf Druckluft basierenden Methode zur Lärmminderung an rotierenden Werkzeugen*, Abschlussbericht zum Forschungsvorhaben HE, 1656/121-2.

[3] STEHLE T., HEISEL U., BIRENBAUM C., 2011, *Simulation und experimentelle Untersuchung von Kreissägeblättern. Holztechnologie*, 52/3, 15-21.

[4] STEHLE T., HEISEL U., BIRENBAUM C., 2013, *Simulative Untersuchung von Kreissägeblättern, wt* Werkstattstechnik online, 103, 1/2, 69-75.

[5] FFOWCS-WILLIAMS J.E., HAWKINGS D.L., 1969, *Sound generation by turbulence and surfaces in arbitrary motion*. Royal Society Publishing London (A), 264, 321-342.

[6] LIGHTHILL M.J., 1952, *On sound generated aerodynamically. I. General theory*, Royal Society Publishing London (A) 222, 564-587.

[7] LIGHTHILL M.J., 1952, *On sound generated aerodynamically. II. Turbulences as a source of sound*, Royal Society Publishing London (A), 222, 1-32.

[8] KÖLTZSCH P., 2004, *Geräuschentstehung durch Strömungen – Grundlagen und Überblick*, Vortrag zur Tagung, Aeroakustik, Haus der Technik Essen, Stuttgart.

[9] BLAGA A., TALPEANU D., STEHLE T., 2015, *Chip loosening factor and chip size distribution during the circular sawing of wood and wood materials*, Holztechnologie, 57/1, 23 -30.